Nanoscale Advances

ROYAL SOCIETY OF CHEMISTRY

PAPER

View Article Online
View Journal | View Issue

Cite this: *Nanoscale Adv.*, 2022, **4**, 4169

An intelligent cooling material modified with carbon dots for evaporative cooling and UV absorption†

Yi Gao,[abc] Shaofeng Liang,[c] Shuangliang Zhao,[abde] Wei Gao, *[abcd] Zequan Li,[c] Muqun Wang,[c] Hong Li,[c] Xiangning He,[c] Riyao Cong,[c] Hailin Diao,[f] Chuwang Su[c] and Xiaoying Xie[abg]

The emergence of cooling technology has brought about huge social benefits to society, but it is also accompanied by the serious problem of energy consumption. In countries close to the equator, intense solar radiation is accompanied by unbearable high temperatures and strong ultraviolet radiation. Therefore, we prepared a simple hydrogel with good evaporative cooling, which can work continuously and has good UV absorption, to solve the indoor cooling and UV radiation problems. Polyacrylamide (PAM) in the hydrogel provides a mechanically strong backbone, and polyethylene glycol (PEG) slows water loss and provides the hydrogel with the ability to reflect infrared light. Lithium bromide (LiBr) is a highly efficient water vapor absorbent, which can provide the hydrogel with water regeneration capability. Carbon dots (CDs) can provide excellent UV absorption for hydrogels, and CDs (4.28 kJ kg^{-1} K^{-1}) have a higher specific heat capacity than water (4.20 kJ kg^{-1} K^{-1}), which can store more heat for a better indoor cooling effect. The composite hydrogel has a good prospect of application in the windows of residential and high-rise buildings.

Received 15th June 2022
Accepted 10th August 2022

DOI: 10.1039/d2na00380e

rsc.li/nanoscale-advances

Introduction

In modern society, refrigeration technology seems to have become ubiquitous. And it is considered by some scholars to be one of the most revolutionary engineering achievements of the century.[1] There is no doubt that refrigeration technology brings about enormous social benefits. Although refrigeration technology has brought about great social benefits, this technology is also accompanied by energy consumption and environmental concerns. It is worth noting that the total greenhouse gas emissions from refrigeration amount to 7.8% in the whole world.[2] The energy consumed by building cooling accounts for a large and growing percentage of the energy consumed by all refrigeration projects.[3] For overall building cooling, windows are one of the most used and least energy consuming components in operation. The temperature regulation of the building interior through windows is a very effective way.[4] It is of great significance to apply energy-saving refrigeration technology to windows to achieve indoor cooling and energy saving.[5,6] Therefore, the combination of simple structural design and evaporative refrigeration is a highly desirable way, albeit challenging, to achieve this.[7–9]

At the same time, UV radiation is also a concern, as almost 9% of the Earth's solar energy is in the UV region.[10] The risks of exposure to solar ultraviolet radiation (UVR) have long been known. Therefore, the World Health Organization (WHO) has recommended that people living in areas between 30°N and 30°S need year-round sun protection.[11] Even indoors, UV radiation can still cause harm to humans through windows, so regulating UV radiation through windows is a good solution.[12,13] Carbon dots (CDs) are a new type of carbon nanomaterial with a unique structure that has excellent absorption of UV light.[14–18] The application of CDs to windows can well solve the indoor problem of ultraviolet radiation.

Liu reported a layer-by-layer (LBL) structure including a silica aerogel layer and an extra phase change material layer was designed. This structure demonstrates a dual-function regulation performance that regulates and equalizes cold (−30 °C) and hot (70 °C) environments.[19] Huang *et al.* developed

[a]*Key Laboratory of Disaster Prevention and Structural Safety of Ministry of Education, Guangxi University, Nanning 530004, Guangxi, China. E-mail: galaxy@gxu.edu.cn*
[b]*Guangxi Key Laboratory of Disaster Prevention and Engineering Safety, Guangxi University, Nanning 530004, Guangxi, China*
[c]*School of Resources, Environment and Materials, Guangxi University, Nanning 530004, Guangxi, China*
[d]*Guangxi Engineering and Technology Research Center for High Quality Structural Panels from Biomass Wastes, Nanning 530004, Guangxi, China*
[e]*College of Chemistry and Chemical Engineering, Guangxi University, Nanning 530004, Guangxi, China*
[f]*Forestry College, Guangxi University, Nanning 530004, Guangxi, China*
[g]*School of Civil Engineering and Architecture, Guangxi University, Nanning 530004, Guangxi, China*

† Electronic supplementary information (ESI) available. See https://doi.org/10.1039/d2na00380e

a surfactant-assisted ball milling method to prepare an aqueous P(VDF-HFP) coating. The coating was 9.5 °C cooler than room air and 6.2 °C cooler than paint at a solar flux of 950 W m^{-2} compared with a common titanium dioxide-based paint, further demonstrating the better cooling ability of the aqueous P(VDF-HFP) coating.[20] Fang reported the tuneable sunlight scattering behavior of a thermochromic hydrogel. The hydrogel moderator can maintain its own temperature difference within 1.2 °C at ambient air temperature differences exceeding 6 °C.[21] In the past, scholars have reported these thermoregulators as a coating or a combination device. In particular, this paper pioneered the introduction of carbon dots with UV absorbing function into hydrogels. This carbon dot hydrogel offers different advantages at the same time.

In this work, we prepare a hydrogel with acrylamide (AM) and polyethylene glycol (PEG) as a simple design of the cooling system, and the hydrogel has good cooling performance. Lithium bromide (LiBr) can provide regeneration capability for the hydrogel and the regeneration time can be shortened with increasing concentration of LiBr. After loading CDs into the hydrogel, the hydrogel has excellent UV shielding ability, which can well solve the UV radiation problem, and CDs have higher specific heat capacity than water, which can help the hydrogel to store more heat and achieve a better indoor cooling effect.

Experimental section

Materials

Magnolia leaves (picked from Guangxi University), ethanol (99.7%, Macklin), acrylamide (AM, 99%, Aladdin), poly(ethylene glycol) (PEG, average M_n 20 000, Aladdin), *N*,*N*-methylenebis (acrylamide) (MBA, 99%, Macklin), 2-hydroxy-4′-(2-hydroxyethoxy)-2-methylpropiophenone (I2959, 98% (HPLC), Aladdin), lithium bromide (LiBr, 99%, Macklin), and polymethyl methacrylate board (20 cm × 20 cm × 5 mm) were used in this study.

Synthesis of carbon dots

The synthesis method of red fluorescent CDs was as follows: (1) Magnolia leaves were chosen as the biomass carbon source, 1 g of leaves was taken and cut up; (2) 5 mL of mixed solution (the volume ratio of ethanol to water was 4 : 1) was added, and the mixture was ground well, and placed in a centrifuge, rotated at 8000 rpm, and centrifuged for 8 min and the supernatant was taken; (3) the supernatant was placed in an autoclave at a temperature of 180 °C and heated for 12 hours to ensure sufficient carbonization; (4) the solution was dialyzed using a dialysis bag (MD25-3000) for 48 h to obtain the desired CD solution; (5) the solution was freeze-dried to obtain a powder for the next step of characterization.

Synthesis of the hydrogel

Synthesize of the hydrogel: (1) 2.6 g AM and 0.4 g PEG_{20000} were taken in a beaker, 30 mL DI water was added and dissolved fully; (2) then 0.13 g MBA (crosslinker) and 780 mg I2959 (photoinitiator) were added and dissolved fully; (3) an ultraviolet lamp (365 nm, 45 w) was used for irradiation, and the curing time was 1 h. In addition, we also synthesized hydrogels with different raw material ratios to facilitate comparison and selection, and the material ratio table is shown in Table 1.

Table 1 Different monomer ratios of the hydrogel

Named	AM (g)	PEG_{20000} (g)	MBA (g)	I2959 (g)
Hydrogel-0	3.0	0.0	0.15	0.090
Hydrogel-1	2.8	0.2	0.14	0.084
Hydrogel-2	2.6	0.4	0.13	0.078
Hydrogel-3	2.4	0.6	0.12	0.072
Hydrogel-4	2.2	0.8	0.11	0.066
Hydrogel-5	2.0	1.0	0.10	0.060

CDs-hydrogel: after the hydrogel was fully swelled in water, it was placed in an oven for dehydration, and the dehydrated hydrogel was placed in CDs (1 mg mL^{-1}) to swell again, and CDs-hydrogel was obtained.

LiBr-hydrogel: after the hydrogel was completely dehydrated in an oven (50 °C), it was immersed in LiBr. When the hydrogel was completely absorbed and swelled, LiBr-hydrogel was obtained.

CDs/LiBr-hydrogel: LiBr was dissolved in CDs (1 mg mL^{-1}), the completely dehydrated hydrogel was immersed in it, and the hydrogel was left to be completely swollen by absorbing water, and then CDs/LiBr-hydrogel was obtained.

Characterization

TEM was performed by using a 300 kV field emission transmission electron microscope (FEI TECNAI G2 F30, FEI); electron transition was performed by using a UV-Vis spectrophotometer (Agilent 8453, Agilent); functional group testing was performed by FTIR (Nicolet IS 50, Thermo Fisher); fluorescence spectroscopy was performed by using a fluorescence spectrophotometer (CARY ECLIPSE, Agilent). A compression test was performed by using a universal testing machine (ZQ-990A, ZHIQU). The reflectance was measured by using a UV-visible NIR spectrometer (UV-3600Plus, Shimadzu) and a near infrared spectrum analyzer (TANGO-R, Bruker). The specific heat capacity was measured by using a thermal conductivity meter (TPS 2500S, Hot Disk), and the UV radiation test was performed by using a UV illuminance meter (TM213, TENMARS).

Windows were assembled with PMMA sheets and the hydrogel was placed in the middle like a "sandwich" structure of a smart window. Smart windows were assembled on a simulated building and it was placed outdoors. The building was simulated under both daytime and night-time conditions to test the cooling performance and the ability of the hydrogel to block UV light.

Results and discussion

The prepared CDs were characterized, using TEM to observe the CDs, which showed a sphere-like morphology with good dispersion in Fig. 1a. The chemical bonds in CDs and maximum emission wavelength are confirmed by UV-vis analysis and a fluorescence spectrometer as shown in Fig. 1b. The typical

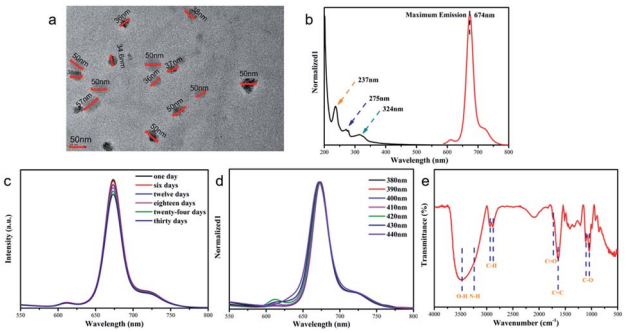

Fig. 1 (a) TEM of CDs; (b) UV-Vis absorbance and fluorescence spectra (the illustration is before and after CDs were irradiated with ultraviolet light); (c) stability of CD solution; (d) different wavelength (380–440 nm) FL emission spectra; (e) FTIR.

absorption peak of CDs at 237 nm belongs to the $\pi \rightarrow \pi^*$ transition in the cores, and the absorption peak at 275 nm belongs to the $n \rightarrow \pi^*$ transition of C=O.[19] The third absorption at about 324 nm originates from the $n \rightarrow \pi^*$ edge transition.[20] According to the fluorescence spectrum, the maximum emission wavelength of CDs is 674 nm. As shown in Fig. S1,† the prepared CD solution was clarified and transparent, and emitted bright red fluorescence under UV light irradiation. As shown in Fig. S2,† the quantum luminescence yield of CDs extracted from fresh Magnolia leaves was 5.8%. To further explore the performance of CDs in practical applications, stability needs to be verified. And as shown in Fig. 1c, upon exposing CDs outdoor for 30 days, CDs maintained good stability with little reduction in fluorescence intensity. Generally, the pH of the solution leads to changes in the luminescence properties of CDs. As shown in Fig. S3(a)†, the pH of the original CD solution was 4. When the pH was increased or decreased, it caused a change in the CD luminescence intensity. Carefully, solutions that are slightly more acidic, neutral and weakly basic can slightly improve the luminescence of CDs in UV light. In particular, when the solution of CDs is more basic, the luminescence of CDs is sharply increased. In order to verify the luminescence stability of the CDs, we placed the CDs under a UV lamp for 90 min and as a result, the luminescence intensity of the CDs decreased by 25%. CDs were excited with a wavelength of 380–440 nm with an interval of 10 nm and the optical behavior of CDs was observed as shown in Fig. 1d. With the increase of the excitation wavelength, the emission peak of CDs did not shift significantly, and CDs showed the characteristic of emission independent excitation in Fig. 1d. The functional groups of CDs are characterized. As shown in the Fourier transform infrared (FT-IR) spectrum in Fig. 1e, the absorption peaks at 3465 cm^{-1} and 3240 cm^{-1} belong to –OH and –NH, respectively.[21] The absorption peaks located at 2942 cm^{-1} and 2875 cm^{-1} belong to the C–H stretching and bending vibrations, respectively.[22,23] The absorption peaks at 1719 cm^{-1} and 1631 cm^{-1} are attributed to the stretching vibration of C=O with C=C.[24,25] Finally, the absorption peaks located at 1115 cm^{-1} and 1036 cm^{-1} belong to the asymmetric and symmetric stretching vibration peaks of C–O, respectively.[26] FT-IR results show that CDs have many active groups and have good water solubility.

Fig. 2a shows the XPS spectrum of CDs, which shows three representative peaks of C1s (285 eV), N1s (400 eV) and O1s (532 eV). The C1s results in XPS contain three different characteristic peaks (Fig. 2b): C=C (284 eV), C=O (285 eV), and HO–C=O (288 eV); In the N1s results of XPS, there are two different characteristic peaks (Fig. 2c): pyridine nitrogen (398 eV) and pyrrolic nitrogen (399 eV); in the O1s results of XPS, there are three different characteristic peaks (Fig. 2d): C–O–C (530 eV), C=O (531 eV), and C–OH (532 eV). The XPS results showed that the CDs contained many reactive functional groups, which was consistent with the FT-IR results.

Due to the existence of C=C, it gives CDs the ability to absorb in the near ultraviolet region.[27] Fig. 3a shows a schematic diagram of the absorption of CDs in the near-UV region. We used UV from 200 to 400 nm for the excitation of CDs, and the CDs responded well to different wavelengths of UV excitation as shown in Fig. 3a. Interestingly, CDs have dual emission under the excitation of ultraviolet light, while most of the CDs reported now have single emission. In addition, Fig. 1d shows that CDs have an absorption response in the blue light region as well. In summary, the CDs prepared from biomass as a precursor can absorb light not only in the near-UV region but also in the visible region. To further apply CDs in practice, we incorporated CDs into hydrogels. CDs-hydrogel was tested outdoors. The UV absorption ability of the hydrogel was tested in both sunny and cloudy weather, and the hydrogel had excellent UV absorption ability and was almost shielded from UV radiation as shown in Fig. 3b–c. The CDs/PEG/PAM hydrogel, as shown in Fig. S4,† can fluoresce blue under UV irradiation, and therefore can be well shielded from UV light. However, considering the factor of cloud obstruction during the test, we choose a 10 mm hydrogel for the next test.

To select the optimal hydrogel, different hydrogels were characterized. As shown in Fig. 4a, the hydrogel without the addition of PEG_{20000} maintains good transparency, while the addition of PEG_{20000} makes the hydrogel appear "whitened",

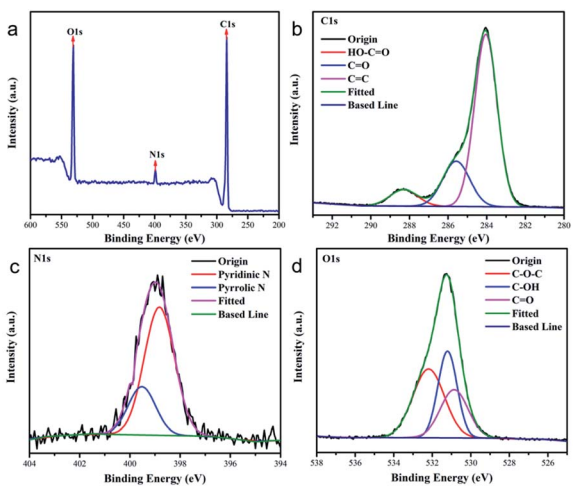

Fig. 2 (a) XPS, (b) C1s, (c) N1s and (d) O1s.

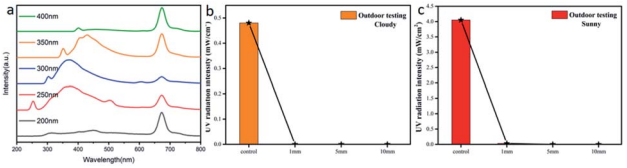

Fig. 3 (a) The excitation response of carbon dots in different wavelength bands in the near ultraviolet region; (b) UV absorption ability of CDs-hydrogel of different thicknesses in outdoor testing (cloudy); (c) UV absorption ability of CDs-hydrogel of different thicknesses in outdoor testing (sunny).

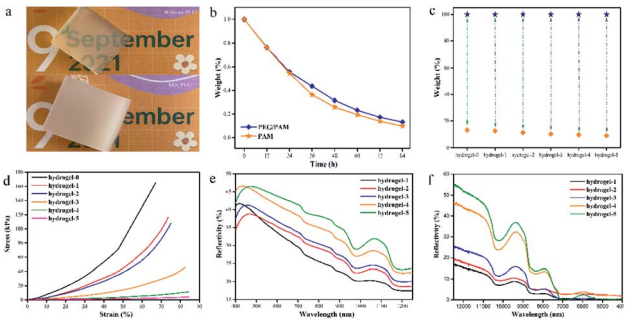

Fig. 4 (a) Photos of hydrogels without PEG_{20000} and with PEG_{20000}. (b) Weight loss of hydrogels without PEG_{20000} and with PEG_{20000} at room temperature. (c) The weight change of different hydrogels before and after drying. (d) Compressive stress–strain curves of different hydrogels. (e) Reflectance curves of different hydrogels (400–1250 nm). (f) Reflectance curves of different hydrogels (4000–12 500 nm).

which provides the hydrogel with the ability to reflect NIR light.[28,29] In addition, polyethylene glycol has excellent moisturizing properties that slow down the loss of water, as shown in Fig. 4b. It also increases the water content of the hydrogel, which can be seen from Fig. 4c, with the increase of the PEG content. To ensure that the hydrogel can be used in life, the hydrogel needs a certain mechanical strength, but polyethylene glycol is a long-chain polymer, which makes the hydrogel lose some of its rigidity as shown in Fig. S5.† Compared to hydrogel-0, the mechanical strength of other hydrogels has decreased, as shown in Fig. 4d. However, both hydrogel-1 and hydrogel-2 were able to maintain their morphology well without deformation under the pressure of 500 g weight, as shown in Fig. S6.† As shown in Fig. S7,† hydrogel-0 and -1 both appeared to be broken after dehydration, while the other hydrogels could still keep their shapes intact after dehydration. The PAM hydrogel is too rigid and will break after complete dehydration, but the softened hydrogel can still maintain the intact form under dehydration. The addition of PEG endows the hydrogel with the ability to reflect light, and it is known from Fig. 4e and f that the reflection of near-infrared light is greater with increasing PEG content. The reflection of near-infrared light can be synergistically cooled down with cooling evaporation.

LiBr is an efficient water vapor absorber and air humidity regulator, loaded into the hydrogel to give the hydrogel the ability to regenerate after water loss.[30] The hydrogel composed of PAM and PEG, which distributes LiBr in the hydrogel, can effectively maintain the water content of the hydrogel, as shown in Fig. 5a–c. With the synergistic effect of PEG and LiBr, the hydrogel is less susceptible to water loss, which is essential for the cooling system. In addition, the hydrogel needs to have good regeneration ability. We placed the hydrogel outdoors and after two hours of exposure to sunlight, the hydrogel lost nearly 10% of its weight. Then, the hydrogel was placed in a room and the hydrogel was regenerated by absorbing water from the air after the temperature dropped, and after 10 hours, the hydrogel was completely regenerated, as shown in Fig. 5d. However, an excessively long regeneration time is clearly inappropriate. Increasing the concentration of LiBr can accelerate the regeneration of the hydrogel and thus shorten the regeneration time as shown in Fig. 5e. Fig. 5f and g show the time for a hydrogel to lose 0.1 g of water at 55 °C and then regenerate at room temperature. The regeneration time decreases with increasing ambient temperature and humidity, which is attributed to high humidity and ambient temperature. High humidity is necessary to accelerate the regeneration time, while an increase in temperature accelerates the movement of molecules and thus the absorption of water from the environment by the hydrogel.

As shown in Fig. 6a, we assembled the windows using PMMA sheets and placed the hydrogel in the middle, like a "sandwich" structure. One side of the PMMA board with holes facilitates the evaporation of water and takes away heat. At the same time, it

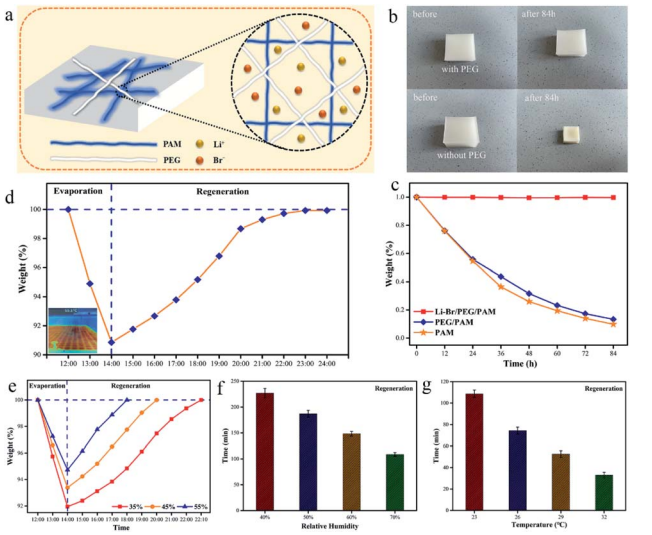

Fig. 5 (a) Schematic structure of LiBr-hydrogel. (b) Photos of the hydrogel without LiBr and with LiBr after 84 h at room temperature. (c) Weight loss of PAM, PAM/PEG and PAM/PEG/LiBr at room temperature. (d) Mass variation of LiBr-hydrogel when heated outdoors and cooled indoors. The indoor temperature is 25 °C. The relative humidity of the indoor environment is 60%. (e) Effect of LiBr concentration on the water regeneration performance of hydrogels. (f) The time required for a hydrogel to lose 0.1 g of water at 55 °C and regain water from the air at an ambient temperature of 23 °C. The relative humidity is 40 to 70%. (g) The time required for the hydrogel to lose 0.1 g of water at 55 °C and regain water from the air at an ambient temperature of 23–32 °C. Relative humidity 70%.

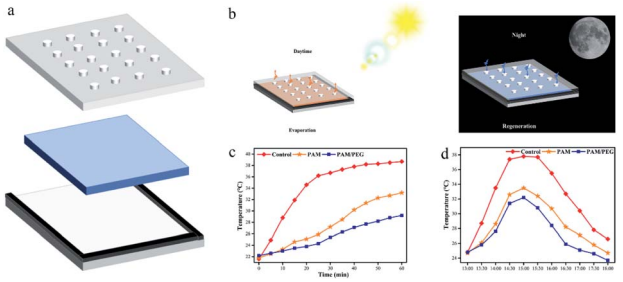

Fig. 6 (a) Smart window assembly diagram. (b) Working principle diagram of the smart window during day and night. (c) Smart window indoor testing. (d) Smart window outdoor testing.

can also effectively protect the hydrogel and play a self-cleaning role. Fig. 6b shows the diurnal working principle of the smart window. During the daytime, the hydrogel is exposed to the radiation of the sun, and the evaporated water escapes through the hole, which acts as evaporative cooling. At night, the moisture in the air is absorbed by the hydrogel through the holes for regeneration. As shown in Fig. S8,† the smart windows were assembled, and indoor simulation tests and outdoor tests were conducted to verify the cooling performance of the hydrogel. Fig. 6c shows the indoor test results of the hydrogel. From the results, the hydrogel can effectively have a cooling effect, and the PAM and PAM/PEG decreased the temperature by 5.5 and 9.5 °C respectively after 60 min of heating by a light source. Due to the presence of a large number of hydrogen bonds in water, water has a high specific heat capacity ($C_p = 4.2$ kJ kg^{-1} K^{-1}), which can effectively store heat.[31,32] As shown in Fig. S9,† the temperature of the hydrogel after heating for 60 min is as high as 56.2 °C. The outdoor test results are shown in Fig. 6d. The temperature of the three groups of test samples peaked after 3 h of sunlight irradiation, and the temperature of PAM and PAM/PEG decreased by 4.3 and 5.6 °C, respectively. The test results show that the hydrogel has excellent cooling performance, and PAM/PEG shows better cooling performance than PAM.

Fig. 7a shows the schematic structure of the composite hydrogel. CDs and LiBr are distributed in the hydrogel, CDs can efficiently absorb UV light, LiBr provides regeneration ability for the hydrogel,[33] and PEG and PAM can lock the water. In Fig. S10,† it is obvious that CDs distribute evenly in the hydrogel network. PAM and PVA provide the skeleton structure of the hydrogel, and the carbon quantum dots are wrapped inside. The hydrogel structure of the double network has good mechanical properties and enough space, as shown in Fig. 1e, because of the presence of C=O in the structure of CDs. In Fig. 7b, the specific heat capacity (4.28 kJ kg^{-1} K^{-1}) of the CDs/PAM/PEG hydrogel is higher than that of water (4.20 kJ kg^{-1} K^{-1}),[34] which means that the thermal storage capacity of the hydrogel is enhanced. The UV absorbing ability of the hydrogel was tested outdoors, and the hydrogel can effectively solve the problem of UV radiation indoors on both sunny and cloudy days as shown in Fig. 7c. The composite hydrogel was tested for outdoor cooling performance, and the results are shown in Fig. 7d. Compared with the blank group, the composite hydrogel decreased by 6.1 °C at most. Compared with the hydrogel without CDs, the composite hydrogel decreased the temperature by 0.5 °C. The results showed that the cooling performance of the composite hydrogel was better. The good UV absorption ability and cooling evaporation performance can make the composite hydrogel have good application prospects. Applying the composite hydrogel to offices, residences, and buildings with floor-to-ceiling windows (cafes) can block ultraviolet rays and reduce cooling energy consumption.

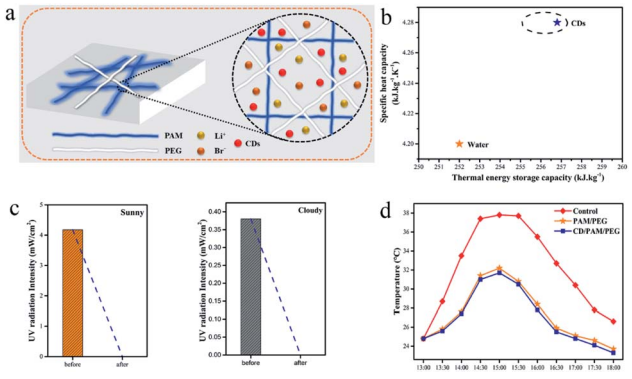

Fig. 7 (a) Schematic structure of CDs/LiBr-hydrogel. (b) Specific heat capacity of CDs and water. (c) UV absorption (sunny & cloudy). (d) CDs/PAM/PEG hydrogel outdoor testing and comparison.

Conclusions

In this work, we built a simple system to solve the indoor cooling and UV radiation problems. The hydrogel consists of PAM and PEG. PAM provides a mechanical framework and can withstand a pressure of 500 g without deformation. PEG "whitened" the hydrogel, allowing it to reflect infrared light. LiBr provides water regeneration ability for the hydrogel, which can recover up to 10% of the lost water within ten hours. Therefore, long-term evaporative cooling can be maintained. We also introduced CDs into the hydrogel to provide effective UV absorption to the hydrogel. The introduction of CDs also improved the thermal storage capacity of the composite hydrogel. The specific heat capacity (4.28 kJ kg^{-1} K^{-1}) of the CDs/PAM/PEG hydrogel is higher than that of water to achieve better room cooling. Compared with the blank group, the PAM/PEG decreased the temperature by up to 6.1 °C. And the hydrogel containing CDs lowered the temperature by 0.5 °C more. Therefore, the good UV absorption and evaporative cooling of CDs/PAM/PEG gels can be well applied to residential windows, as well as glazing and floor-to-ceiling windows in some high-rise buildings.

Author contributions

Yi Gao: conceptualization; methodology; validation; writing – original draft preparation; Shaofeng Liang: conceptualization; methodology; validation; writing – review & editing; Shuangliang Zhao: writing – review & editing; Wei Gao: project administration; supervision; resources; funding acquisition;

Zequan Li: validation; writing – review & editing; Muqun Wang: validation; writing – review & editing; Hong Li: writing – review & editing; investigation; Riyao Cong: writing – review & editing; Xiangning He: writing – review & editing; investigation; Hailin Diao: review & editing; Chuwang Su: review & editing; Xiaoying Xie: review & editing.

Conflicts of interest

There are no conflicts to declare.

Acknowledgements

This work was supported by the Key R&D projects in Guangxi (AB21196033), Chongzuo Science and Technology planning project (FA2017005), Interdisciplinary Scientific Research Foundation of Guangxi University (Grant No. 2022JCC017), and the Industry-university Research Cooperation Fund of Guangxi Jinding Furniture Group Co., Ltd & Guangxi University (20200820).

Notes and references

1 G. Constable, B. Somerville and J. Lienhard, *Phys. Today*, 2004, **57**, 63.
2 M. O. McLinden, C. J. Seeton and A. Pearson, *Science*, 2020, **370**, 791–796.
3 C. Z. Feng, P. H. Yang, H. D. Liu, M. R. Mao, Y. P. Liu, T. Xue, J. Fu, T. Cheng, X. J. Hu, H. J. Fan and K. Liu, *Nano Energy*, 2021, 85.
4 M. Tarantini, A. D. Loprieno and P. L. Porta, *Energy*, 2011, **36**, 2473–2482.
5 T. Miyazaki, A. Akisawa and I. Nikai, *Energy Build.*, 2011, **43**, 2211–2218.
6 P. M. Cuce and S. Riffat, *Renewable Sustainable Energy Rev.*, 2016, **54**, 1240–1249.
7 S. Cui, C. Ahn, M. C. Wingert, D. Leung, S. Cai and R. Chen, *Appl. Energy*, 2016, **168**, 332–339.
8 R. Y. Li, Y. S. Shi, M. C. Wu, S. Y. Hong and P. Wang, *Nat. Sustain*, 2020, **3**, 636–643.
9 C. X. Wang, L. J. Hua, H. Z. Yan, B. J. Li, Y. D. Tu and R. Z. Wang, *Joule*, 2020, **4**, 435–447.
10 E. Monroy, F. Omnes and F. Calle, *Semicond. Sci. Technol.*, 2003, **18**, R33–R51.
11 P. Gies and J. Wright, *Photochem. Photobiol.*, 2003, **78**, 342–348.
12 L. L. Wu, H. J. Fang, C. Zheng, Q. Wang and H. Wang, *J. Mater. Chem. C*, 2019, **7**, 10446–10453.
13 V. K. Baliyan, K. U. Jeong and S. W. Kang, *Dyes Pigm.*, 2019, **166**, 403–409.
14 B. K. Barman, T. Nagao and K. K. Nanda, *Appl. Surf. Sci.*, 2020, 510.
15 D. Y. Zuo, N. Liang, J. Xu, D. Z. Chen and H. W. Zhang, *Cellulose*, 2019, **26**, 4205–4212.
16 X. Feng, Y. F. Zhao, Y. Q. Jiang, M. Miao, S. M. Cao and J. H. Fang, *Carbohydr. Polym.*, 2017, **161**, 253–260.
17 S. J. Park, H. K. Yang and B. K. Moon, *Nano Energy*, 2019, **60**, 87–94.
18 S. Liang, M. Wang, W. Gao, S. Luo, N. Huang and Y. Qin, *Carbon Trends*, 2021, **4**, 100063.
19 L. Liu, X. Shan, X. Hu, W. Lv and J. Wang, *ACS Nano*, 2021, **15**, 19771–19782.
20 W. Huang, Y. Chen, Y. Luo, J. Mandal, W. Li, M. Chen, C. C. Tsai, Z. Shan, N. Yu and Y. Yang, *Adv. Funct. Mater.*, 2021, 31.
21 Z. Fang, L. Ding, L. Li, K. Shuai, B. Cao, Y. Zhong, Z. Meng and Z. Xia, *ACS Photonics*, 2021, **8**, 2781–2790.
22 L. B. Tang, R. B. Ji, X. K. Cao, J. Y. Lin, H. X. Jiang, X. M. Li, K. S. Teng, C. M. Luk, S. J. Zeng, J. H. Hao and S. P. Lau, *ACS Nano*, 2012, **6**, 5102–5110.
23 C. J. Reckmeier, Y. Wang, R. Zboril and A. L. Rogach, *J. Phys. Chem. C*, 2016, **120**, 10591–10604.
24 P. J. Yang, J. H. Zhao, L. X. Zhang, L. Li and Z. P. Zhu, *Chem.–Eur. J.*, 2015, **21**, 8561–8568.
25 T. L. Feng, Q. S. Zeng, S. Y. Lu, X. J. Yan, J. J. Liu, S. Y. Tao, M. X. Yang and B. Yang, *ACS Photonics*, 2018, **5**, 502–510.
26 X. Miao, D. Qu, D. X. Yang, B. Nie, Y. K. Zhao, H. Y. Fan and Z. C. Sun, *Adv. Mater.*, 2018, 30.
27 H. Ding, S. B. Yu, J. S. Wei and H. M. Xiong, *ACS Nano*, 2016, **10**, 484–491.
28 H. Ding, J. S. Wei and H. M. Xiong, *Nanoscale*, 2014, **6**, 13817–13823.
29 D. Li, D. Han, S. N. Qu, L. Liu, P. T. Jing, D. Zhou, W. Y. Ji, X. Y. Wang, T. F. Zhang and D. Z. Shen, *Appl. Phys. Lett.*, 2016, 5.
30 F. L. Yuan, T. Yuan, L. Z. Sui, Z. B. Wang, Z. F. Xi, Y. C. Li, X. H. Li, L. Z. Fan, Z. A. Tan, A. M. Chen, M. X. Jin and S. H. Yang, *Nat. Commun.*, 2018, 9.
31 X. Y. Li, J. Peoples, P. Y. Yao and X. L. Ruan, *ACS Appl. Mater. Interfaces*, 2021, **13**, 21733–21739.
32 J. Mandal, Y. Yang, N. F. Yu and A. P. Raman, *Joule*, 2020, **4**, 1350–1356.
33 S. R. Pu, Y. T. Liao, K. L. Chen, J. Fu, S. L. Zhang, L. R. Ge, G. Conta, S. Bouzarif, T. Cheng, X. J. Hu, K. Liu and J. Chen, *Nano Lett.*, 2020, **20**, 3791–3797.
34 K. A. T. Silverstein, A. D. J. Haymet and K. A. Dill, *J. Am. Chem. Soc.*, 2000, **122**, 8037–8041.